Molecular Modeling Connect
ISSN: 3105-3734
2026, Vol. 3, Cite as: doi:10.x/journal.x.x.x

SCIFINITI PUBLISHING

OPEN ACCESS

Research Article

Computational Exploration of Mutant SARS-CoV-2 Main Protease as a Target for Binding and Inhibition Attributes Utilizing Antiviral Drugs for Therapeutic Application

Sudheer Kumar Katari[1*#], Chandu Sai Kanakala[1#], Anil Kumar Singh[2*#]

[1]Department of Biotechnology, Vignan's Foundation for Science, Technology and Research, Vadlamudi-522213, Guntur, India

[2]Academy of Scientific and Innovative Research (AcSIR), Ghaziabad-201002, India.

*Corresponding authors: katari319@gmail.com (S.K. Katari); phd.anil@yahoo.com (A.K.Singh);

# equally contributed to this work.

2026, Vol. 3
doi:10.x/journal.x.x.x

Highlights

- Selected antiviral agents were evaluated against the mutant Mpro of SARS-CoV-2.
- Docking simulation exhibited best binding affinity for Indinavir with a binding affinity of -8.07±0.06 Kcal/mol, along with a *K*i of 1.21μM.
- Desmond MD Simulation exhibited P-L stability during a 100 ns duration under NPT ensemble.
- Computational results affirm the adequate binding and inhibitory capability of the evaluated antiviral drugs for the repurposing towards Mpro inhibition.

Abstract

Mutations in the main protease (Mpro) of SARS-CoV-2 have resulted in resistance to available inhibitors and various other compounds that have been reported. Targeting the inhibition of SARS-CoV-2 Mpro presents a promising opportunity to develop potent therapeutic agents aimed at combating SARS-CoV-2 and similar viruses. The presented study evaluates a selection of ten antiviral agents—Acyclovir, Remdesivir, Sofosbuvir, Atazanavir, Cidofovir, Indinavir, Lopinavir, Oseltamivir, Galidesivir, and Favipiravir—focusing on their ability to bind and inhibit mutant Mpro through various computational methods. The computational physical-chemical properties and secondary structure elements (SSE) exhibit comparable values between WT and mutant variants of Mpro. The Mpro-Indinavir docked complex was identified as the high-ranked docked compound, with a binding affinity of -8.07±0.06 Kcal/mol and a *K*i value of 1.21 μM. This docked complex was involved hydrogen bond interactions between the THR-26 and GLN-189 residues. The binding affinity of all docked compounds was found to be in a range from -5.37± 0.40 to -8.07±0.06 Kcal/mol. The

docked complexes underwent a thorough assessment through a 100 ns MD simulation, which confirmed the stability of the top-ranked docked complexes. The findings indicate that some antiviral agents exhibit adequate binding affinity and inhibitory effectiveness, as predicted by *K*i. However, theoretical findings necessitate the subsequent experimental validation. This suggests that compounds with notable binding and other properties can be effectively repurposed as promising therapeutic candidates for Mpro inhibition targeting mutant variants.

Keywords: molecular docking; main protease; binding affinity; inhibition constant; MD simulation

1. Introduction

In late 2019, a highly transmissible and pathogenic coronavirus, known as severe acute respiratory syndrome coronavirus 2 (SARS-CoV-2), was emerged, leading to a global pandemic of acute respiratory disease recognized as “coronavirus disease 2019” (COVID-19). This infection triggers a threat to public safety and human health [1]. The COVID-19 pandemic accounted for over 18 million mortality and substantially destabilized the world economy, with continuing repercussions [2]. As a consequence of the rapid evolutionary nature, the global viral population has noticed a significant increase in the frequency of dozens of mutations, including those that enhance its transmissibility and enable it escape human immune responses [3]. The estimated mutation rate for SARS-CoV-2 is around 1×10^{-6}–2×10^{-6} mutations per nucleotide per replication cycle, which is in line with earlier estimates for other betacoronaviruses [4]. Antigenic drift, on the other hand, causes Omicron subvariants to change continuously, which is challenging because it makes vaccines less effective and could alter susceptibility to antiviral agents [5]. According to reports, four antivirals—

ensitrelvir (S-217622), nirmatrelvir (PF-07321332), remdesivir (GS-441524), and molnupiravir (EIDD-1931)—have been approved for the treatment of SARS-CoV-2 infections [5-9]. Among such, Ensitrelvir and nirmatrelvir inhibit the viral 3C-like (3CL) protease (Mpro), which is a conserved enzyme that is necessary for polyprotein cleavage and viral replication. On the other hand, remdesivir and molnupiravir block the RNA-dependent RNA polymerase (RdRp), which stops viral genome replication [5]. Resistance mutations, particularly in Mpro, have emerged as these antivirals are utilized more frequently in clinical contexts, which has led to concerns regarding their long-term efficacy [5]. Although Mpro is a highly conserved protease found in many coronaviruses, no human proteases have comparable cleavage specificity. Therefore, Mpro is an appealing prime target for antiviral drug research for COVID-19 treatment [10]. Moreover, a key benefit of focusing on Mpro is its conserved nature across coronaviruses. Despite the genetic variation present within the coronavirus family, Mpro exhibits significant sequence and structural similarities between strains. Nirmatrelvir, an approved treatment option for COVID-19, binds covalently to the active site cysteine of the SARS-CoV-2 Mpro. This action effectively blocks enzyme activity and halts viral replication, an approved treatment option for COVID-19, binds covalently to the active site cysteine of the SARS-CoV-2 Mpro. This action effectively blocks enzyme activity and halts viral replication [11]. It inhibits viral polyprotein processing, which eventually leads to the cessation of viral replication, by binding covalently and in a reversible manner to the cysteine that is located in the active site of Mpro of SARS-CoV-2 [11]. It has been shown that the influence of nirmatrelvir pressure may cause proximal and active-site mutation in the Mpro of SARS-CoV-2. These mutations reduce the efficacy of the drug and contribute to Paxlovid resistance

[11]. As a consequence of this, six Mpro mutations evolved, each of which included T304I either by itself or in combination with T21I, L50F, T135I, S144A, or A173V. Among these, the A173V+T304I and T21I+S144A+T304I mutations exhibited resistance to Nirmatrelvir that was >20-fold [12]. Alongside the aforementioned antiviral agents, Remdesivir, Hydroxychloroquine, Favipiravir, Lopinavir, and Ritonavir have been commonly utilized in the treatment of COVID-19 [9, 13-15]. Furthermore, reports on HIV protease inhibitors reported that those could be effective in the treatment of COVID-19 as novel strategies [16-19]. The effectiveness of these drugs in combating COVID-19 can differ, depending on their capacity to effectively bind to the SARS-CoV-2 protease, a substantial molecule made up by the coronavirus as it replicates within the human body. To facilitate the advancement of future antiviral drugs for SARS-CoV-2, it is vital to determine the binding affinities of novel compounds, including antivirals, against the mutant form of SARS-CoV-2 Mpro. The present study evaluated the structural and functional attributes of the SARS-CoV-2 Mpro mutant variant using multivalent computational techniques. A selection of ten established antiviral agents was screened against the mutant Mpro to determine their binding affinity and inhibition potential, with the goal of gaining deeper insights into the inhibitory effects of these agents. The computational findings revealed that SARS-CoV-2 Mpro protein exhibited sufficient binding affinities and inhibitory characteristics associated with certain antiviral agents. However, the experimental or in vitro validation is still necessary to support the computational results in the search for novel strategies for dealing with the newly emerged SARS-CoV virus in the future.

2. Methods

2.1 Selection and optimization of antiviral agents

A set of ten well-known antiviral agents was selected (Table 1), based on recently published literature [20-27]. Structural files in 2D coordinates of selected antiviral drugs were acquired from the PubChem database (https://pubchem.ncbi.nlm.nih.gov) [28]. All retrieved antiviral drugs (ligands) were optimized for energy minimization using the MMFF94 force field in the Avogadro tool (Version 1.2.0) [29, 30]. Further, pH for human physiological conditions (pH 7.4 ± 0.5) was set up during ligand preparation for molecular docking by correcting ionization state, tautomers, and stereoisomers, to ensure accurate binding affinity and ligand conformation in the receptor (Protein).

2.2 Protein crystal structure of SARS-CoV-2 M^{pro} preparation and refinement

Recent findings indicate that mutations in Mpro result in resistance to nirmatrelvir, a recognized inhibitor. For this investigation, the protein crystal structure of SARS-CoV-2 Mpro with a mutation was employed. This was retrieved using PDB ID: 9AUK from the Protein Data Bank (https://www.rcsb.org) [12, 33]. The sequence length was 306 residues distributed over two chains (A and B). The 9AUK protein model was solved by X-ray diffraction; Resolution: 1.88 Å; R-Value Free: 0.253; R-Value Work: 0.207, and R-Value Observed: 0.210 [12]. This had a mutation as (A173V). The structure followed a thorough refining procedure, during which existing ligands, co-crystals, and water molecules were removed. Subsequently, the receptor was carefully set up for the docking simulation by adding polar hydrogen, correcting the side chain, and performing energy minimization.

2.3 Structural and physico-chemical property assessment of the main protease

Structural analyses of two variants of SARS-CoV-2 Mpro, as non-mutant and mutant, were performed by accessing their constituents' amino acid residues. PDBs as 6Y2E and 9AUK were used for structural overlay using needleman-wunsch algorithm, BLOSUM62 matrix with a cutoff distance of 2Å. Secondary structural elements (SSEs) were also calculated to determine the difference in SSE components using an online resource (https://npsa.lyon.inserm.fr/cgi-bin/npsa_automat.pl?page=/NPSA/npsa_sopma.html). The molecular weight, predicted pI, amino acid/atomic makeup, extinction coefficient, instability index, aliphatic index, and GRAVY are some of the most important key physical and chemical factors from a protein sequence that were predicted. It checks for stability, hydrophobicity, and solubility characterization. To compare the physico-chemical parameters of both Mpro, the Expasy-ProtParam web tool was deployed for both wild and mutant variants.

2.4 Molecular docking to explore binding affinity and molecular interactions assessment

The refined protein structure of SARS-CoV-2 mutant Mpro (PDB ID: 9AUK) was utilized in docking analyses with selected optimized ligands. Docking was conducted in GUI mode using the PyRx program (v. 0.8), which integrated AutoDock Vina. A grid box with dimensions of 71 × 74 × 54 Å (X, Y, Z coordinates) was used to allocate the 3D search space on the refined Mpro protein, where the ligands would bind. The binding energies are shown by Vina, where the highest-ranking binding free energy always corresponds to a 0 RMSD. When comparing each ligand to the reference compound, the binding free energy was taken into account as the same with 0 RMSD values. The bound complex post-docking was meticulously analyzed for potential

hydrogen bond interactions and key amino acid residues within the active site, utilizing UCSF Chimera X and the Discovery Studio visualizer (v 16.1.0.15350) software [32, 33].

2.5 Inhibition constant (*K*i) calculation

After docking inhibition constant (*K*i) was calculated from the final Gibbs free energy of binding (ΔG) by implementing the following formula: $Ki = \exp(\Delta G/RT)$, where R is the universal gas constant (1.985×10^{-3} kcal mol^{-1} K^{-1}) and T is the temperature (298.15 K). *K*i was employed to predict the effectiveness of inhibitors (Docked ligands).

2.6 Validation of docked complexes to get insight into stability and structural changes by Desmond MD simulation

Docking is not effective enough for assuming various parameters of structural and functional conformational changes. MD simulation was conducted using Desmond v2024.4 to explore changes in the conformation of the protein–ligand complex within the solvent system [34]. The OPLS forcefield was employed within an orthorhombic cubic box, centering the complex while filling the space with TIP3P water molecules and buffers, maintaining a distance of 10 Å [34]. The system was neutralized by adding ions, such as Na+ and Cl−, to the boundary condition box volume in a random manner [34]. The MD simulation was conducted under the isothermal isobaric ensemble (NPT) with a temperature of 310 K, pressure of 1 atm, and thermostat relaxation time of 200 ps. The Nosé-Hoover thermostat and the Martyne–Tobias—Klein barostat approaches were employed to maintain the pressure and temperature scale at 310 K and 1 atm, respectively, during MD simulations [35]. The 100 ns NPT phase serves as a crucial period for data collection, enabling the observation of stable

molecular behavior, protein conformational changes, and ligand-binding interactions on a 100 ns scale. Post simulation parameters were evaluated for depth analyses and conclude the findings.

3. Results

3.1 Structural and physico-chemical property assessment of the main protease

Three-dimensional structures contain essential information for visualizing structural attributes, regardless of the presence of bound ligands. The 3D structures of SARS-CoV-2 Mpro non-mutant and mutant were predicted using the coordinates file (PDB ID: 6Y2E, 9AUK). The structures were further compared with structural alignment, represented in cartoon style (Figure 1). SSE was outlined with similar values for three variants as 24.18% (Helix), 28.76% (Sheet), and 47.06% (Coil). In addition, both variants were assessed for various physical and chemical properties predicted by ProtParam. Almost comparable molecular weight was highlighted due to similar constituent amino acid residues (306 for both variants), as 33796.64 (Da) for the non-mutant and 33824.69 (Da) for the mutant. Negatively charged residues (Asp + Glu) in both variants were found to be 26, while positively charged residues (Arg + Lys) were counted as 22. Not much significant difference was found in other parameters, as listed in Table 2.

3.2 Molecular docking to explore binding affinity, and molecular interactions assessment: post-docking analyses

The binding affinities and potential molecular interactions between mutant Mpro-antiviral agents were investigated using docking. Each docked complex was evaluated separately for binding affinity, crucial active site residues involved in H-bond

interactions, and the results were reported in mean ± SD, n = 3. The Mpro-Indinavir complex exhibited the lowest binding affinity at -8.07±0.06 Kcal/mol when compared to the reference (Nirmatrelvir). Key interacting residues consist of THR-26 and GLN-189, which are involved in an H-bond interaction. The Mpro-Sofosbuvir complex exhibited a binding affinity of -7.50±0.26 Kcal/mol, indicating a relative second rank among all docked complexes. This complex is involved with the residues HIS-41, GLY-143, SER-144, CYS-145, and HIS-163 through the formation of H-bonds. Detailed docking findings have been listed in Table 3. The docking assessment revealed that the binding energy of each ligand exhibited notable variation, ranging from -5.37± 0.40 to -8.07±0.06 Kcal/mol. Figure 2 portrays the top four binding affinity complexes featuring 2D interactions.

3.3 Inhibition constant (*K*i) calculation

In the present study, *K*i was used to determine how well a ligand binds to a target to exert inhibitory action. It was calculated as the concentration required to produce half-maximum inhibition. Calculated *K*i from estimated free binding energy (ΔG); a lower *K*i value can define a stronger binding with significant potency. The best-ranked docked complex, Mpro-Indinavir, possessed a *K*i concentration value of 1.21 μM to inhibit the Mpro mutant, acting as an inhibitor with a *K*i measured as high as 115.00 μM for Favipiravir. *K*i for each antiviral was predicted to be distinct from 1.21 to 115.00 μM (Table 3).

3.4 Validation of docked complexes to get insight into stability and structural changes by Desmond MD simulation

Four top-ranked docked complexes underwent a 100 ns MD simulation to assess the stability of the complexes and to analyze the fluctuations in the protein associated with the docked ligand. A few key parameters listed below are described in detail.

3.4.1 Protein-ligand RMSD analyses

The protein–ligand complexes were simulated for 100 ns to assess stability and protein fluctuations with bound ligands. The RMSD of carbon alpha (Cα) atoms was computed to assess the comprehensive structural changes and deviations of the complexes (Protein-Ligand) throughout the simulation. The average RMSD value was observed to be <2.5 Å for all top four docked complexes. Top-ranked complex Mpro-Indinavir exhibited stability at the end of simulation with an average RMSD of 2.1Å (Figure 3-A). Second-ranked complex Mpro- Sofosbuvir exhibited stability at the end (beyond 60ns) of the simulation with an average RMSD of 2.1Å (Figure 3-B). Mpro-Lopinavir exhibited stability from 0 to 100 ns with an average RMSD of 2.0 Å (Figure 3-C). Last-ranked complex Mpro-Atazanavir exhibited instability with ligand till the end of the simulation run with an average RMSD of 2.2 Å (Figure 3-D).

3.4.2 Protein RMSF analyses

An RMSF investigation was performed to assess the fluctuations of proteins that occur when they are bound to ligands. The RMSF values for each protein residue throughout the simulation period provide insightful details about the mobility and flexibility of the residues. According to the predicted RMSF values, the majority of protein residues exhibited little change throughout the simulation, remained less than 1.5. Å. Mpro-Indinavir complex observed for an average RMSF value of 1.0 Å. The highest fluctuation was observed within GLY-302 (6.8Å), SER-301 (5.0 Å), and CYS-300 (3.8

Å) residues (Figure 4-A). Mpro- Sofosbuvir complex observed for an average RMSF value of 1.1 Å. Highest fluctuation were observed within SER-1(5.2 Å), GLY-302 (5.5 Å), SER-301(3.3Å) residues (Figure 4-B). Mpro-Lopinavir complex observed for an average RMSF value of 1.1 Å. Highest fluctuation were observed within GLY_302 (4.5 Å), GLY_2(3.4 Å), SER_301(2.7 Å) residues (Figure 4-C). Mpro-Atazanavir complex was found to have the highest fluctuation in SER_1 (6.1 Å), GLY_2 (4.7Å), GLY_302 (4.6Å) residues with an average RMSF value of 1.1 Å (Figure 4-D).

3.4.3 Protein-Ligand contacts analyses

Protein-ligand interactions were examined for binding stability, revealing hydrogen bonding. Interaction histograms and 2D maps reveal residue-specific frequency throughout the trajectory. The Mpro-Indinavir complex reveals that the residues THR-199, TYR-237, ASN-238, TYR-239, LEU-271, LEU-272, ASN-274, MET-276, ASN-277, GLY-278, ALA-285, LEU-287, and GLU-288 engage in formation of H-bond contacts (Figure 5- A). The Mpro- Sofosbuvir complex reveals that the residues GLN-19, THR-24, THR-26, ASN-28, HIS-41, SER-46, TYR-118, ASN-119, GLY-120, ASN-142, CYS-145, HIS-164, GLU-166, and GLN-189 engage in formation of H-bond contacts (Figure 5-B). The Mpro-Lopinavir complex revealed that the residues PHE-3, TRP-207, MET-276, ASN-277, GLY-278, ARG-279, LEU-286, LEU-287, and GLU-288 were engaged in H-bond interactions (Figure 5-C). Last fourth ranked complex, Mpro-Atazanavir complex, revealed that the residues HIS-80, LYS-90, LYS-236, TYR-237, ASN-238, TYR-239, LEU-271, LEU-272, GLN-273, ASN-274, GLY-275, MET-276 were engaged in H-bond interactions (Figure 5-D).

3.4.4 Post-simulation energy assessment

Analyzing potential energy after simulations in Desmond is essential for evaluating system stability, the quality of equilibration, and the structural energy landscapes. This analysis was conducted with the help of Schrödinger's Maestro interface tools following the completion of MD simulations. Post simulation P_E was assessed in a range of -119333.748 to -127536.512 Kcal/mol. The comparative plot of P_E is depicted in Figure 6.

4. Discussion

The structural and functional characteristics of a protein play a vital role in defining its biological properties. The protein-ligand complexes that achieve the highest scores indicate the potential for off-target interactions of the ligand. The active site residues of a protein or receptor play a crucial role in the binding of drugs (ligands). In fact, these active site residues serve as the crucial molecular framework for ligand interaction. The Mpro stands out as a vital target for exploring inhibitors intended for combating COVID-19. In recent years, a multitude of studies have documented the existence of potential inhibitors that target Mpro [36-38]. For example, Nirmatrelvir, the pioneering oral Mpro inhibitor for treating severe COVID-19 cases, faces challenges in effectiveness due to evolved mutations in Mpro, which have been associated with resistance to Nirmatrelvir [39]. Considering the likelihood of unexpected toxicity associated with covalent inhibitors due to their high reactivity, it is crucial to focus on the development of noncovalent inhibitors for SARS-CoV-2 Mpro [10, 40]. In this scenario, the discovery of a potential molecule might be beneficial in addressing future challenges associated with COVID-19. This present study examined ten antiviral agents targeting the SARS-CoV-2 Mpro mutant variant to understand the binding affinity of these agents as potential therapeutic options. Computational physical-

chemical properties exhibited comparable parameters, which further concluded that non-mutant and mutant variants have similar values in predicted parameters, i.e., Theoretical pI, Instability index, Aliphatic index, and a few others, as listed in Table 2. In addition to this, SSE pointed out that both of the Mpro variants had similar values for helix, sheet, and coil, ranging from 24.18% to 47.06%. This might possibly be due to a similar and the same number of constituent amino acid residues. The selected antiviral agents exhibited a notable binding affinity score compared to the reference compound (Nirmatrelvir), standing out among all ligands (antiviral compounds). The Mpro-Indinavir complex revealed the lowest binding affinity among all docked complexes, achieving a remarkable score of -8.07±0.06 Kcal/mol. This complex engaged in H-bond interactions with THR-26 and GLN-189 residues. Conversely, a relatively weak binding affinity was noted for the Mpro-Favipiravir complex, which had a binding affinity score of -5.37± 0.40 (Kcal/mol), including GLN-110, THR-111, ASN-151, ASP-295, and ARG-298 residues, involved in H-bond interactions. Further *K*i, was calculated to estimate the concentration required by the ligand to inhibit Mpro. *K*i for top ranked complex was estimated as 1.21 µM, while 115.00 µM for Favipiravir. The range of *K*i was estimated in a range of 1.21 µM to 115.00 µM. Active site residues such as ARG, LYS, PHE, LEU, GLY, SER, CYS, GLU, THR, ASN, ASP, HIS, TYR, GLN, and MET played a crucial role in H-bond formation within the Mpro-antivirals. Beyond the binding affinity and *K*i, docked complexes were further validated through 100 ns simulation to capture structural conformational information and stability assessment. The top four best-ranked complexes were evaluated to assess P-L RMSD, Protein RMSF, Protein-ligand contacts, and post simulation analyses. Among all, only three complexes had archived stability till the simulation end with an average

RMSD less than 2.2 Å. Amino acid residues that were implicated in H-bond contacts were included PHE, GLN, THR, ASN, HIS, SER, LYS, TYR, GLY, CYS, GLU, TRP, LEU, MET, ARG, and ALA. Further post-simulation P_E energy was also assessed to conclude the simulation. The findings revealed that a few antiviral agents have the capacity to bind to Mpro and inhibit it at precise concentrations in the form of *K*i. This might be used to repurpose antiviral drugs as potent Mpro inhibitors. Furthermore, appropriate experimental studies can be undertaken to validate computational findings as a viable therapeutic option in the treatment of future viruses with features similar to SARS-CoV-2.

5. Conclusion

The structure of proteins serves as a binding framework for target ligands or therapeutic candidates, enabling the modification of the natural activities of associated proteins. Consequently, the structure of proteins provides a conceptual foundation for understanding ligand binding to determine inhibition potential. The presented study carried theoretical exploration with structural analyses, uncovering potent binding affinity attributes for the inhibitory effects of selected antiviral agents on mutant Mpro. The binding affinity was observed with a range that varied from -5.37± 0.40 to -8.07±0.06 Kcal/mol, while the *K*i values were noted to be between 1.21 to 115.00 µM for the selected antiviral agents. The binding affinity and *K*i effectively validated the appropriate binding mechanism and inhibitory concentration in µM. Subsequently, MD simulations revealed stable ligand interactions over a duration of 100 ns. Binding affinity is an important way to screen antiviral agents on mutant Mpro, but further *in vitro* or cell line experimental validation must be conducted to further examine these candidates from other perspectives. The computational findings discussed

could pave the way for repurposing antiviral agents, transforming them into effective therapeutics against mutant Mpro of SARS-CoV-2 and similar emerging viruses in the future.

List of Abbreviations:

Main Protease (Mpro)

Secondary Structure Elements (SSE)

Severe Acute Respiratory Syndrome Coronavirus 2 (SARS-CoV-2)

Coronavirus Disease 2019" (COVID-19)

Author contributions

SKK: Conceptualization, Data curation, Formal analysis, Investigation, Methodology, Validation, Software, Writing–original draft, Writing – review & editing, and Supervision. CSK: Data curation, Formal analysis, Investigation, Methodology, Validation, Software, Writing – review & editing. AKS: Conceptualization, Data curation, Formal analysis, Investigation, Methodology, Validation, Software, Project administration, Writing–original draft, Writing – review & editing, visualisation and Supervision.

Conflicts of interest

The authors confirm that no conflict of interest exists regarding this work.

Availability of data and materials

All data used in the present study were generated from computational experiments and are provided in this paper, and further may be requested from the corresponding authors.

Funding

No funding was available to support this study.

Acknowledgment

SKK is highly thankful to VFSTR (Deemed to be University) for providing the faculty seed grant (F.No. VFSTR/REG/A6/30/2023-24/01 dated 16-05-2023). AKS thankfully acknowledges the “Academy of Scientific and Innovative Research (AcSIR)”, Ghaziabad, India (An Institute of National Importance)

AI-Declaration

No AI-generated text, figures, or data have been used in this research manuscript; all are original content of the authors generated by computational experiments.

References

1. Hu, B., et al., *Characteristics of SARS-CoV-2 and COVID-19.* Nature Reviews Microbiology, 2021. **19**(3): p. 141-154.
2. Zagórska, A., et al. *Inhibitors of SARS-CoV-2 Main Protease (Mpro) as Anti-Coronavirus Agents*. Biomolecules, 2024. **14**.
3. Haddox, Hugh K., et al., *The mutation rate of SARS-CoV-2 is highly variable between sites and is influenced by sequence context, genomic region, and RNA structure.* Nucleic Acids Research, 2025. **53**(11): p. gkaf503.
4. Markov, P.V., et al., *The evolution of SARS-CoV-2.* Nature Reviews Microbiology, 2023. **21**(6): p. 361-379.
5. Min, S.C., et al., *A SARS-CoV-2 Mpro mutation conferring ensitrelvir resistance paradoxically increases nirmatrelvir susceptibility.* Nature Communications, 2025. **16**(1): p. 10737.

6. Mukae, H., et al., *Ensitrelvir as a novel treatment option for mild-to-moderate COVID-19: a narrative literature review.* Therapeutic Advances in Infectious Disease, 2025. **12**: p. 20499361251321724.
7. Jayk Bernal, A., et al., *Molnupiravir for Oral Treatment of Covid-19 in Nonhospitalized Patients.* New England Journal of Medicine, 2022. **386**(6): p. 509-520.
8. Hammond, J., et al., *Oral Nirmatrelvir–Ritonavir as Postexposure Prophylaxis for Covid-19.* New England Journal of Medicine, 2024. **391**(3): p. 224-234.
9. Beigel, J.H., et al., *Remdesivir for the Treatment of Covid-19 — Final Report.* New England Journal of Medicine, 2020. **383**(19): p. 1813-1826.
10. Okabe, A., et al., *Discovery of Highly Potent Noncovalent Inhibitors of SARS-CoV-2 Main Protease through Computer-Aided Drug Design.* Journal of Medicinal Chemistry, 2025. **68**(20): p. 21330-21345.
11. Fischer, C., et al., *Structural insights into the nirmatrelvir-resistant SARS-CoV-2 Mpro L50F/E166A/L167F triple mutant-inhibitor-complex reveal strategies for next generation coronaviral inhibitor design.* RSC Medicinal Chemistry, 2025. **16**(10): p. 5032-5040.
12. Zhu, Y., et al., *In vitro selection and analysis of SARS-CoV-2 nirmatrelvir resistance mutations contributing to clinical virus resistance surveillance.* Science Advances, 2024, **10**(30): p. eadl4013.
13. Cavalcanti, A.B., et al., *Hydroxychloroquine with or without Azithromycin in Mild-to-Moderate Covid-19.* New England Journal of Medicine, 2020. **383**(21): p. 2041-2052.

14. Jorge, A., *Hydroxychloroquine in the prevention of COVID-19 mortality.* The Lancet Rheumatology, 2021. **3**(1): p. e2-e3.
15. Dabbous, H.M., et al., *Efficacy of favipiravir in COVID-19 treatment: a multi-center randomized study.* Arch Virol, 2021. **166**(3): p. 949-954.
16. Ma, L., et al., *Repurposing of HIV/HCV protease inhibitors against SARS-CoV-2 3CLpro.* Antiviral Research, 2022. **207**: p. 105419.
17. von Hentig, N., *Repositioning HIV protease inhibitors and nucleos(t)ide RNA polymerase inhibitors for the treatment of SARS-CoV-2 infection and COVID-19.* European Journal of Clinical Pharmacology, 2021. **77**(9): p. 1297-1307.
18. Yu, W., et al. *Computational Simulation of HIV Protease Inhibitors to the Main Protease (Mpro) of SARS-CoV-2: Implications for COVID-19 Drugs Design*. Molecules, 2021. **26**, 7385.
19. Majerová, T. and J. Konvalinka, *Viral proteases as therapeutic targets.* Molecular Aspects of Medicine, 2022. **88**: p. 101159.
20. Mahdi, M., et al., *Analysis of the efficacy of HIV protease inhibitors against SARS-CoV-2's main protease.* Virology Journal, 2020. **17**(1): p. 190.
21. Sultan, A., et al., *Anti-HIV and anti-HCV small molecule protease inhibitors in-silico repurposing against SARS-CoV-2 Mpro for the treatment of COVID-19.* Journal of Biomolecular Structure and Dynamics, 2021: p. 1-15.
22. Cao, B., et al., *A Trial of Lopinavir–Ritonavir in Adults Hospitalized with Severe Covid-19.* New England Journal of Medicine, 2020. **382**(19): p. 1787-1799.
23. German, E.R., M.K. Jairath, and J. Caston, *Treatment of Long-Haul COVID Patients With Off-Label Acyclovir.* Cureus, 2023. **15**(4): p. e37926.

24. Roozbeh, F., et al., *Sofosbuvir and daclatasvir for the treatment of COVID-19 outpatients: a double-blind, randomized controlled trial.* J Antimicrob Chemother, 2021. **76**(3): p. 753-757.

25. Celik, I., M. Erol, and Z. Duzgun, *In silico evaluation of potential inhibitory activity of remdesivir, favipiravir, ribavirin and galidesivir active forms on SARS-CoV-2 RNA polymerase.* Molecular Diversity, 2022. **26**(1): p. 279-292.

26. Rahman, M.R., et al., *Identification of potential antivirals against SARS-CoV-2 using virtual screening method.* Informatics in Medicine Unlocked, 2021. **23**: p. 100531.

27. Chaves, O.A., et al., *Atazanavir Is a Competitive Inhibitor of SARS-CoV-2 M(pro), Impairing Variants Replication In Vitro and In Vivo.* Pharmaceuticals (Basel), 2021. **15**(1).

28. Kim, S., et al., *PubChem in 2021: new data content and improved web interfaces.* Nucleic Acids Res, 2021. **49**(D1): p. D1388-d1395.

29. Halgren, T.A., *MMFF VI. MMFF94s option for energy minimization studies.* Journal of Computational Chemistry, 1999. **20**(7): p. 720-729.

30. Hanwell, M.D., et al., *Avogadro: an advanced semantic chemical editor, visualization, and analysis platform.* Journal of Cheminformatics, 2012. **4**(1): p. 17.

31. Berman, H.M., et al., *The Protein Data Bank.* Nucleic acids research, 2000. **28**(1): p. 235-242.

32. Studio, D., *BIOVIA, Dassault Systèmes, [Discovery Studio], [v 16.1.0.15350], San Diego: Dassault Systèmes, [2021].*

33. Pettersen, E.F., et al., *UCSF ChimeraX: Structure visualization for researchers, educators, and developers.* Protein Science, 2021. **30**(1): p. 70-82.

34. P, G. and K. M. K, *Docking studies and molecular dynamics simulation of triazole benzene sulfonamide derivatives with human carbonic anhydrase IX inhibition activity.* RSC Advances, 2021. **11**(60): p. 38079-38093.

35. Barrett, T.J. and M.L. Minus, *Nosé-Hoover Integrators at-a-Glance: Barostat Integration Has a Demonstrable Effect on Uniaxial Tension Results of Solid Materials.* Journal of Chemical Theory and Computation, 2025. **21**(2): p. 517-529.

36. Tuttle, J.B., et al., *Discovery of Nirmatrelvir (PF-07321332): A Potent, Orally Active Inhibitor of the Severe Acute Respiratory Syndrome Coronavirus 2 (SARS CoV-2) Main Protease.* Journal of Medicinal Chemistry, 2025. **68**(7): p. 7003-7030.

37. Jin, Z., et al., *Structure of Mpro from SARS-CoV-2 and discovery of its inhibitors.* Nature, 2020. **582**(7811): p. 289-293.

38. Chan, H.T.H., et al., *Discovery of SARS-CoV-2 Mpro peptide inhibitors from modelling substrate and ligand binding.* Chemical Science, 2021. **12**(41): p. 13686-13703.

39. Deschenes, N.M., et al., *Functional and Structural Characterization of Treatment-Emergent Nirmatrelvir Resistance Mutations at Low Frequencies in the Main Protease (Mpro) Reveals a Unique Evolutionary Route for SARS-CoV-2 to Gain Resistance.* The Journal of Infectious Diseases, 2025. **232**(5): p. e789-e798.

40. Zhang, L., et al., *Resistance mechanisms of SARS-CoV-2 3CLpro to the non-covalent inhibitor WU-04.* Cell Discovery, 2024. **10**(1): p. 40.

2026, Vol. 3
doi:10.x/journal.x.x.x

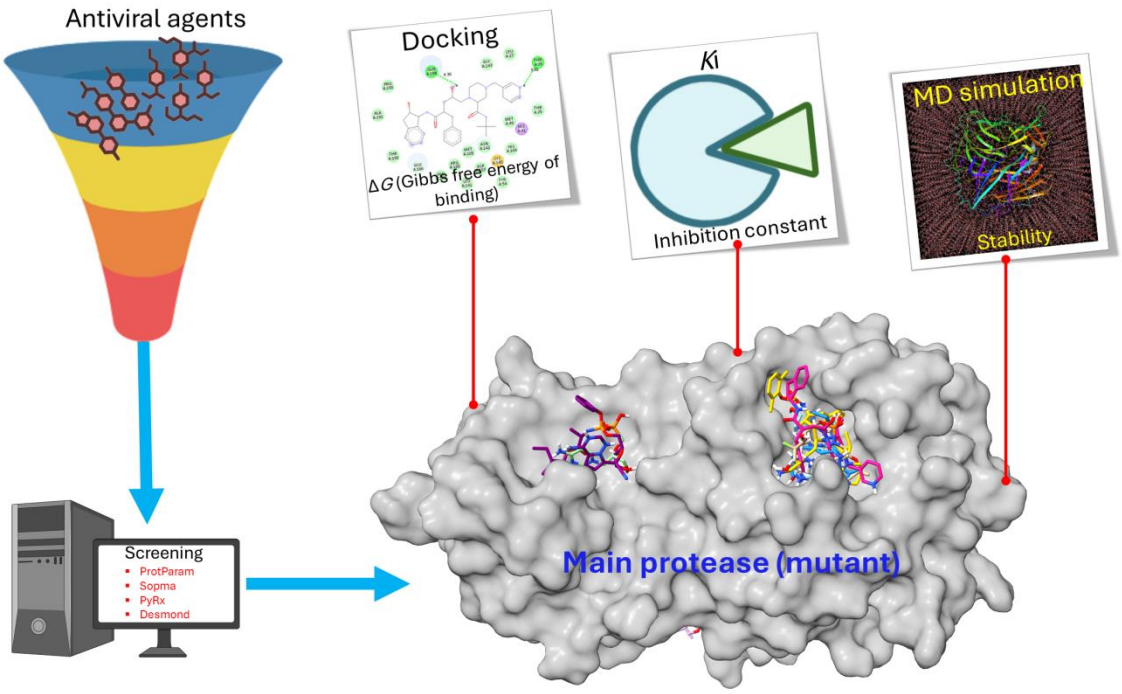

Graphical Abstract

2026, Vol. 3
doi:10.x/journal.x.x.x

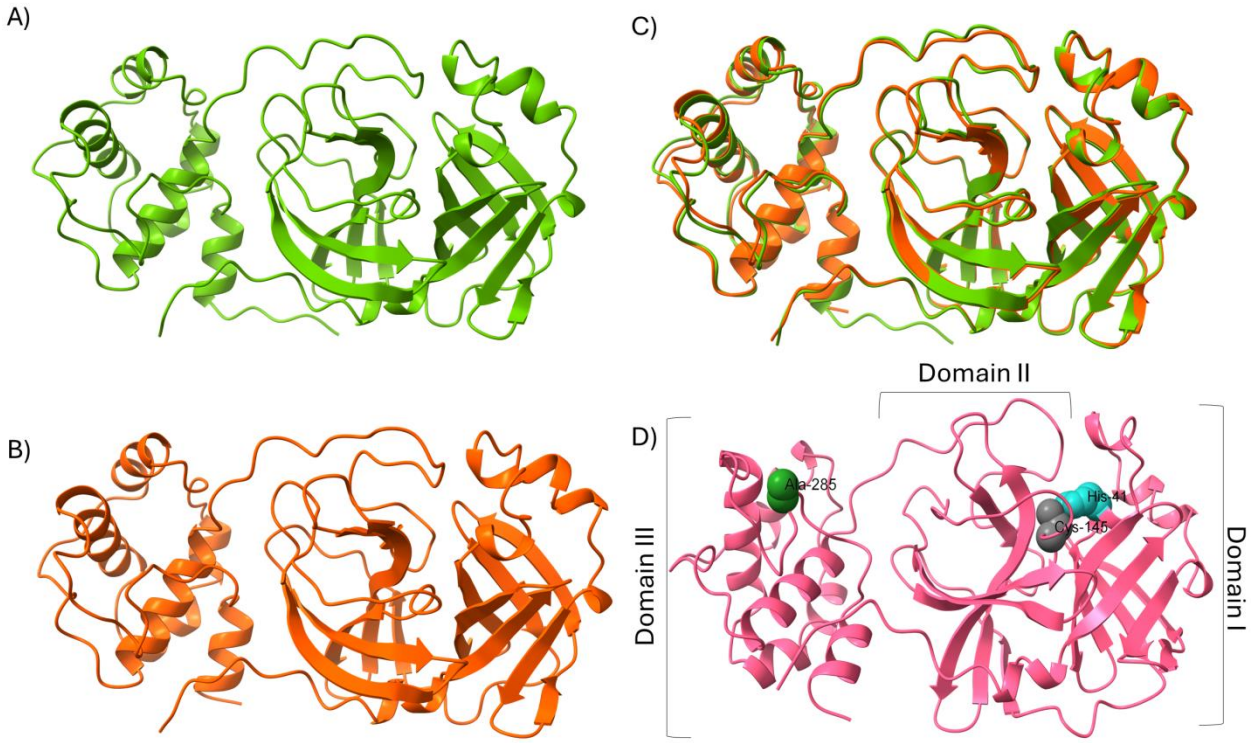

Figure 1: Structural analyses of SARS-CoV-2 Mpro. A) Depiction of a cartoon render of Mpro (WT), image generated from PDB 6Y2E, in a single unit by removing the existing ligand. B) Depiction of a cartoon render of Mpro (Mutant), image generated from PDB 9AUK, in a single unit by removing the existing ligand. C) Depiction of a structure overlay to compare similarity by alignment of residues with an RMSD cutoff value of 2 Å. D) Depiction of a cartoon with marked vital residues present in domains.

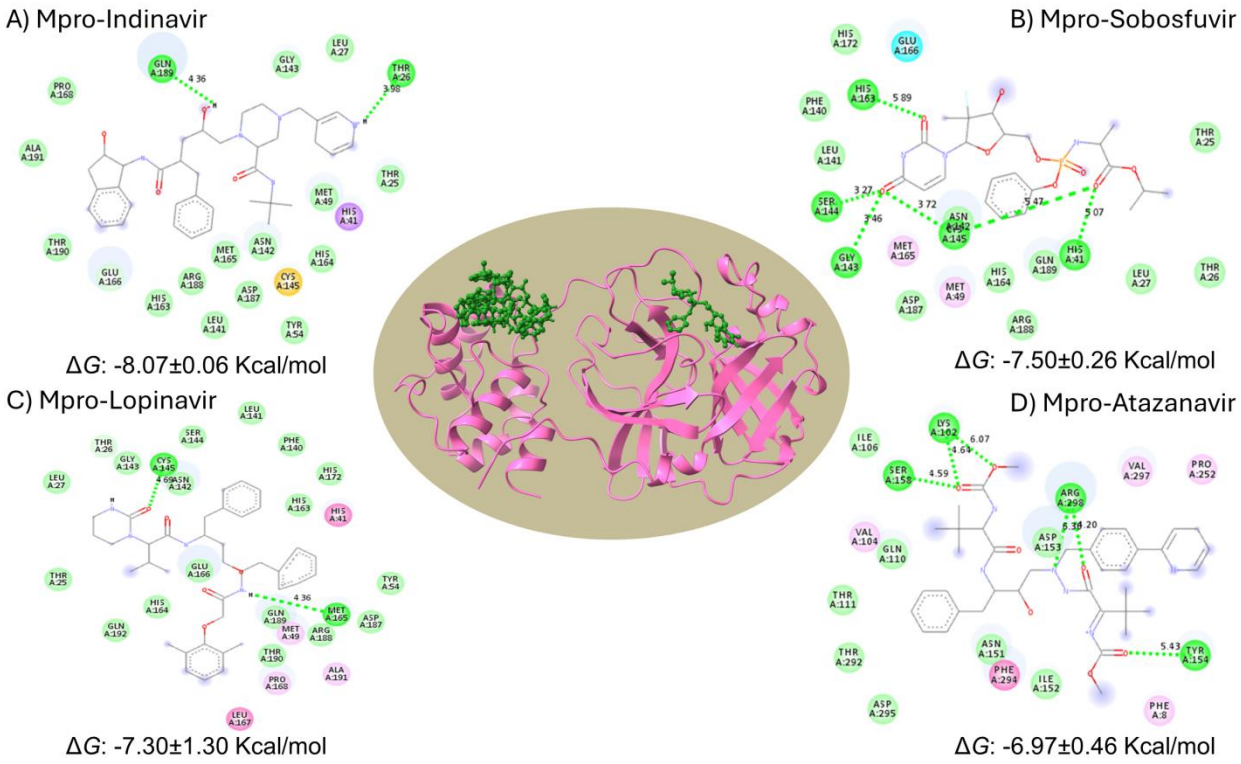

Figure 2: Best-ranked docking pose of ligand-Mpro. The docking pose is marked with an H-bond and bond length. A) 2D interaction of Mpro-Indinavir associated with H-Bond. B) 2D interaction of Mpro-Sofosbuvir associated with H-Bond. C) 2D interaction of Mpro-Lopinavir associated with H-Bond. D) 2D interaction of Mpro-Atazanavir associated with H-Bond.

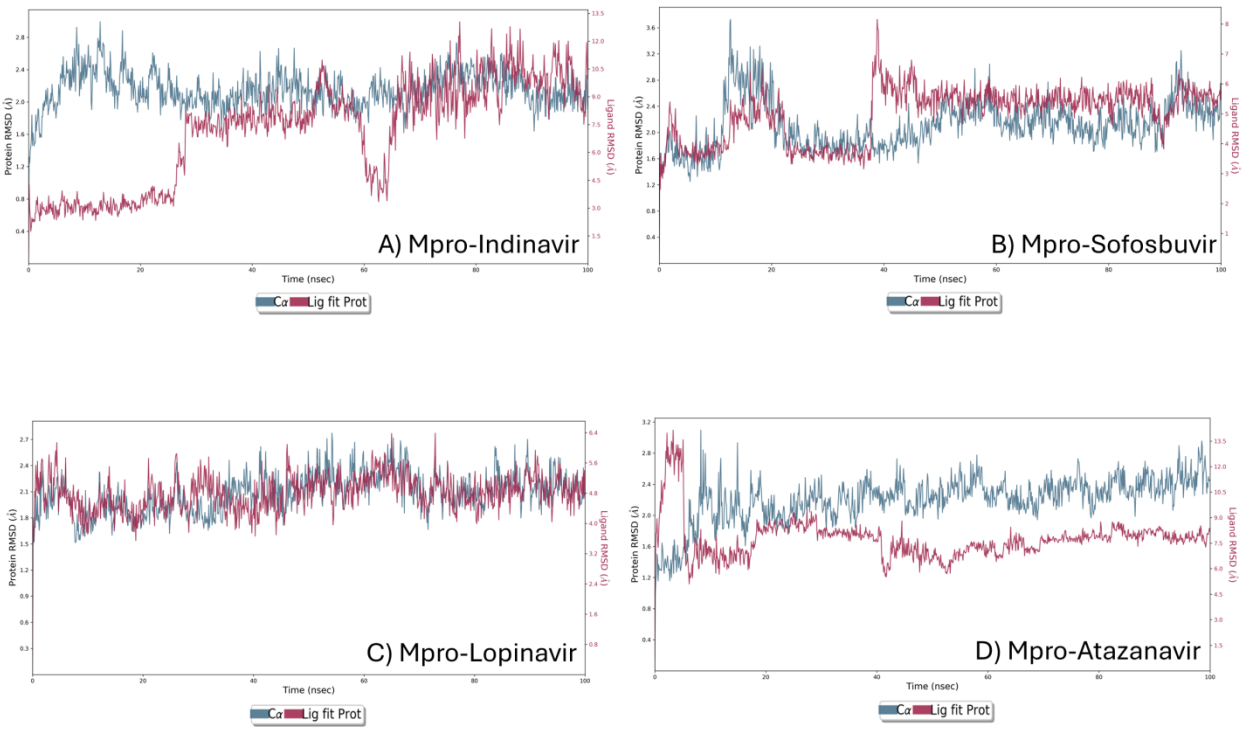

Figure 3: Protein-ligand RMSD plots of top ranked four complexes. A) Portray of Mpro-Indinavir complex RMSD over 100 ns. B) Portray of Mpro-Sofosbuvir complex RMSD over 100 ns. C) Portray of Mpro- Lopinavir complex RMSD over 100 ns. D) Portray of Mpro-Atazanavir complex RMSD over 100 ns. All complexes except C can be observed for system stability at the end of the simulation with an average RMSD of less than 2.5 Å.

2026, Vol. 3
doi:10.x/journal.x.x.x

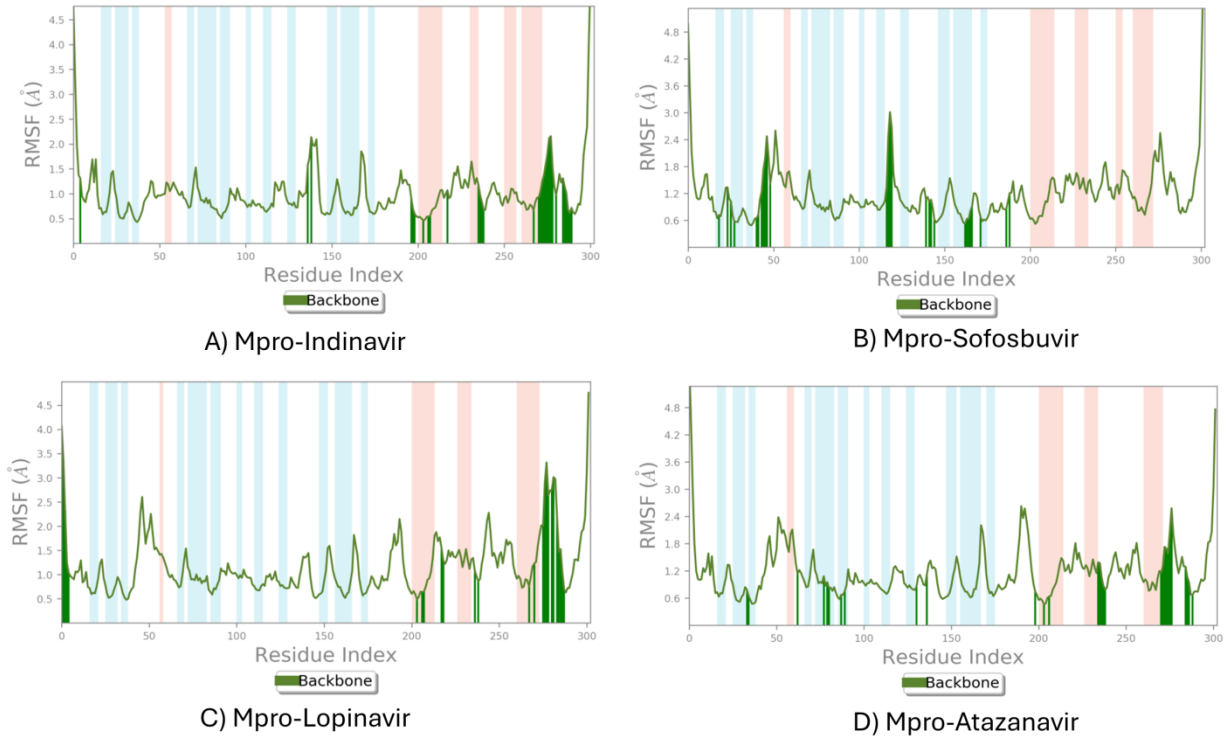

Figure 4: A) Portray of Mpro-Indinavir RMSF plot over 100 ns. B) Portray of Mpro-Sofosbuvir RMSF plot over 100 ns. C) Portray of Mpro-Lopinavir RMSF plot over 100 ns. D) Portray of Mpro-Atazanavir complex RMSF plot over 100 ns.

2026, Vol. 3
doi:10.x/journal.x.x.x

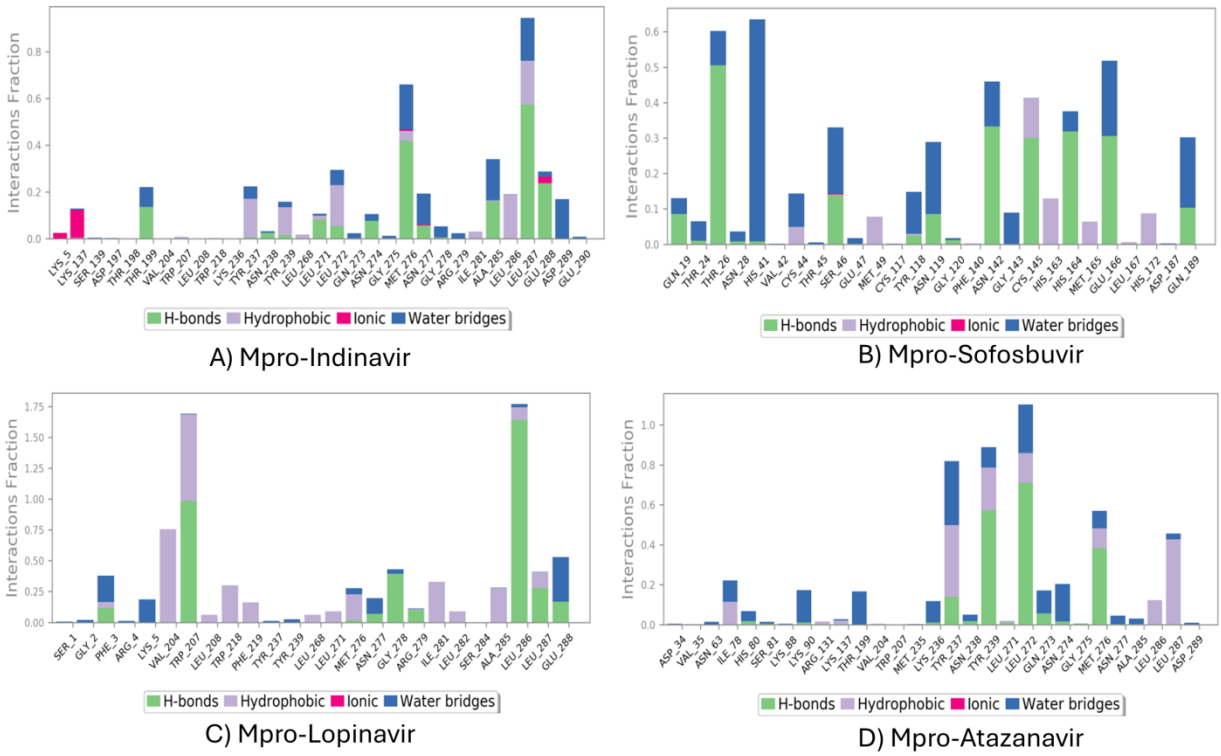

Figure 5: A) Portray of Mpro-Indinavir P-L contacts plot with H-bond interactions among corresponding amino-acid residues. B) Portray of Mpro-Sofosbuvir P-L contacts plot with H-bond interactions among corresponding amino-acid residues. C) Portray of Mpro-Lopinavir P-L contacts plot with H-bond interactions among corresponding amino-acid residues. D) Portray of Mpro-Atazanavir P-L contacts plot with H-bond interactions among corresponding amino-acid residues.

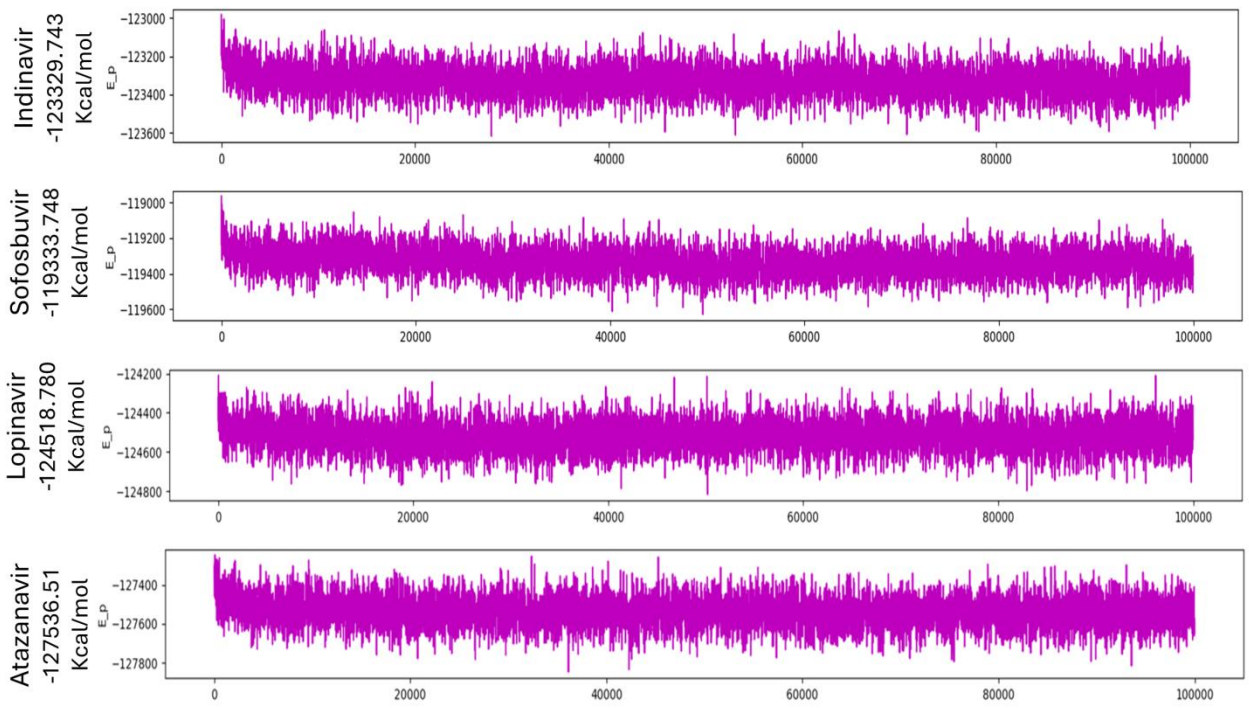

Figure 6: Post-simulation P_E energy plot of the four best-ranked complexes.

2026, Vol. 3
doi:10.x/journal.x.x.x

Table 1: Molecular and chemical attributes of selected antiviral agents for screening binding and inhibition action on mutant main protease (Mpro).

S.NO	Antiviral agent	Molecular depiction in 2D	Molecular weight (g/mol)	Molecular formula
1	Acyclovir	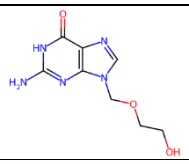	225.20	$C_8H_{11}N_5O_3$
2	Remdesivir	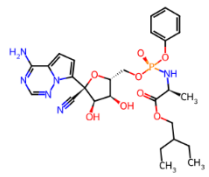	602.6	$C_{27}H_{35}N_6O_8P$
3	Sofosbuvir	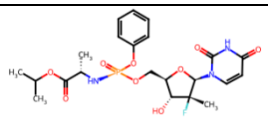	529.5	$C_{22}H_{29}FN_3O_9P$
4	Atazanavir	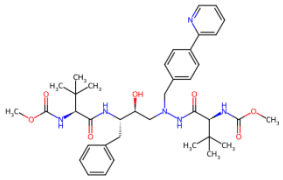	704.9	$C_{38}H_{52}N_6O_7$
5	Cidofovir	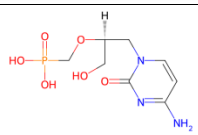	279.19	$C_8H_{14}N_3O_6P$
6	Indinavir	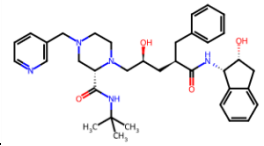	613.8	$C_{36}H_{47}N_5O_4$
7	Lopinavir	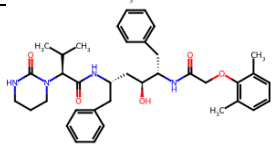	628.8	$C_{37}H_{48}N_4O_5$
8	Oseltamivir		312.40	$C_{16}H_{28}N_2O_4$

9	Galidesivir	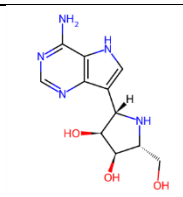	265.27	$C_{11}H_{15}N_5O_3$
10	Favipiravir	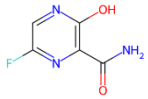	157.10	$C_5H_4FN_3O_2$

Molecular Modeling Connect
ISSN: 3105-3734
2026, Vol. 3, Cite as: doi:10.x/journal.x.x.x

SCIFINITI PUBLISHING

OPEN ACCESS

Research Article

Table 2: Predicted physicochemical and secondary structural analyses.

Parameter		Main protease (6Y2E)	Main protease mutant (9AUK)
Physical and chemical	Residues count	306	306
	Theoretical pI	5.95	5.95
	Molecular weight in Da	33796.64	33824.69
	Molecular formula	$C_{1499}H_{2318}N_{402}O_{445}S_{22}$	$C_{1501}H_{2322}N_{402}O_{445}S_{22}$
	Negatively charged residues (Asp + Glu)	26	26
	Positively charged residues (Arg + Lys)	22	22
	Instability index	27.65	27.37
	Aliphatic index	82.12	82.75
	Grand average of hydropathicity (GRAVY)	-0.019	-0.011
Secondary stru...	Helix	24.18%	24.18%
	sheet	28.76%	28.76%

2026, Vol. 3
doi:10.x/journal.x.x.x

	Coil	47.06%	47.06%

Table 3: Docking analyses of docked antiviral agents to main protease mutant variant with key binding, interacting amino acid residue and Inhibition constant (*K*i).

S.No	Complex (MPro+antiviral)	Binding affinity (Kcal/mol) (Mean ± SD, n = 3)	Interacting amino acid residues	Contact bond type	Inhibition constant (*K*i) µM
1	Acyclovir	-5.57±0.06	PHE-140, LEU-141, GLY-143, SER-144, CYS-145, GLU-166	H-bond	82.4
2	Remdesivir	-6.73±0.31	ARG-131, LYS-137, THR-199, ASN-238, ASP-289	H-bond	11.6
3	Sofosbuvir	-7.50±0.26	HIS-41, GLY-143, SER-144, CYS-145, HIS-163	H-bond	3.16
4	Atazanavir	-6.97±0.46	LYS-102, TYR-154, SER-158, ARG-298	H-bond	7.73
5	Cidofovir	-5.87±0.29	ARG-131, THR-199, ASN-238	H-bond	49.7
6	Indinavir	-8.07±0.06	THR-26, GLN-189	H-bond	1.21
7	Lopinavir	-7.30±1.30	CYS-145, MET-165	H-bond	4.41
8	Oseltamivir	-6.10±0.17	ASN-142, GLY-143, GLU-166	H-bond	33.6
9	Galidesivir	-6.40±0.46	PHE-140, ASN-142, SER-144, CYS-145, HIS-163, GLU-166	H-bond	20.2
10	Favipiravir	-5.37± 0.40	GLN-110, THR-111, ASN-151, ASP-295, ARG-298	H-bond	115.00
*	Nirmatrelvir	-7.80± 0.61	HIS-163, GLU-166, THR-190	H-bond	1.91

* was used as known reference compound.